RESEARCH ARTICLE | FEBRUARY 02 2023

Interface dewetting as a source of void formation and aggregation in phase change nanoscale actuators *⊘*

Xinyi Fang ⁽ⁱ⁾; Mohammad Ayaz Masud ⁽ⁱ⁾; Gianluca Piazza ⁽ⁱ⁾; James Bain ⁽ⁱ⁾

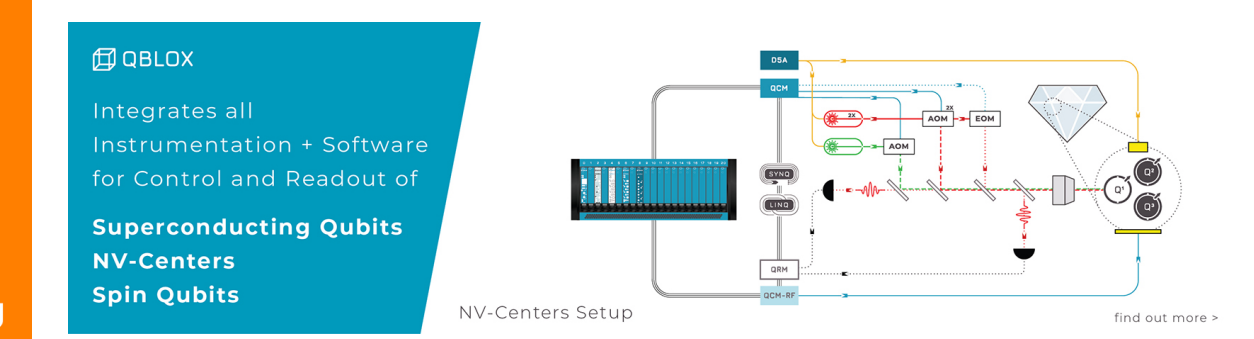


Appl. Phys. Lett. 122, 051602 (2023) https://doi.org/10.1063/5.0137456





CrossMark





Interface dewetting as a source of void formation and aggregation in phase change nanoscale actuators

Cite as: Appl. Phys. Lett. **122**, 051602 (2023); doi: 10.1063/5.0137456 Submitted: 2 December 2022 · Accepted: 18 January 2023 · Published Online: 2 February 2023







Xinyi Fang, 🝺 Mohammad Ayaz Masud, 🕞 Gianluca Piazza, a 🕞 and James Bain a 🕞

AFFILIATIONS

Department of Electrical Engineering and Computer Engineering, Carnegie Mellon University, Pittsburgh, Pennsylvania 15213, USA

^{a)}Authors to whom correspondence should be addressed: piazza@ece.cmu.edu and jbain@cmu.edu

ABSTRACT

This paper reports a phenomenon occurring between phase change material (PCM) germanium telluride (GeTe) and a thin encapsulation layer of alumina when the PCM undergoes the phase transformation, consistent with dewetting of the PCM from the surrounding alumina. Massive structural change, including formation of large voids, which take up to 21.9% of the initial GeTe volume after 10 000 phase change cycles is observed. Electrical and mechanical characterization of the structure confirms this interpretation. A rapid thermal annealing test of blanket films on alumina that demonstrates dewetting further validates this conjecture. The dewetting and associated gross material displacement can lead to an extraordinary actuation corresponding to a one-time 44 nm height change for a 178 nm GeTe thick layer. However, control of this phenomenon is required to build reliable actuators that do not suffer from rupture of the encapsulation layer.

Published under an exclusive license by AIP Publishing. https://doi.org/10.1063/5.0137456

Chalcogenide-based phase change materials (PCMs), such as Ge2Sb2Te5 and GeTe, have been heavily studied and widely used over the past decade owing to their nonvolatile switching behavior between the crystalline phase and amorphous phase. 1-15 The crystalline phase has highly ordered periodic atomic arrangement, while the amorphous phase atoms do not have long-range order. The crystalline to amorphous phase transition, referred to as the "reset" process, is achieved by thermally melting the PCM and quenching it rapidly to prevent rearrangement of the atomic structure. The amorphous to crystalline phase transition, also referred to as the "set" process, requires an annealing temperature below the melting temperature with sufficient time so that the atoms can rearrange into the energetically favorable crystalline configuration. The difference in atomic arrangements gives the two phases attractive material property contrast in optical reflectivity, electrical conductivity, and mechanical density. The high contrast in optical reflectivity allows applications in rewritable optical storage, such as Digital Video Disk and Rewritable Compact Disk, and emerging applications in optical communications, such as nonvolatile waveguides and photonic memories.²⁻⁵ The enormous contrast in electrical conductivity allows development of nonvolatile phase change random access memories,6 which are being investigated for use in neuromorphic computing circuits, ⁷⁻⁹ and high frequency RF switches. ^{10,11} The density change makes PCMs also remarkably interesting for designing

nanoscale actuators. Among all the chalcogenide-based PCMs, GeTe has the greatest density change between the amorphous and crystalline states, close to 8%, ¹² and a corresponding work density of 100 J/cm³, which is one of the highest ever reported for any actuator materials. ¹³ The density change induced by a volumetric change of GeTe has been harnessed to build the liner stressor for FinFETs¹⁴ and the phase change nanomechanical relay (PCNR), ¹⁵ a device that relies on mechanical actuation through GeTe phase transformation and which is the focus of this work.

In this work, we report and explain the experimental evidence that the net actuator displacement upon cycling between the two phases of GeTe can exceed the expected 8% (under the idealized conditions of expansion in only one dimension) and reach 24.7% of the initial height of the PCNR test structure. In fact, it is observed that the encapsulation layer continuously deforms during the phase change cycling and the relative height change, defined as the cap maximum height change in the crystalline GeTe state, reaches 45.6% on average. This very large actuation and cap layer deformation have never been reported before. Analysis of a specifically designed test structure was performed to investigate the mechanism behind this unexpectedly large actuation displacement. The test structure was based on a simplified PCNR structure without the top metallic and source/drain contacts for ease of optical observation of the GeTe behavior through the

transparent alumina encapsulation [shown schematically in Fig. 1(a)]. Endurance cycling test is conducted, and intermediate states are characterized to study the progress of the device deformation. One cycle is defined as two distinct heating cycles, encompassing the volume changes from the crystalline phase (c-GeTe) to the amorphous phase (a-GeTe) and back to c-GeTe. Different structures with different dimensions of the functional GeTe volume and heater are designed to examine the impact of temperature gradients and encapsulation stiffness, which have all been previously reported as affecting the behavior of the PCM, ^{16–20} as well as the dewetting force, which has not been reported as a design variable before.

The basic test structure [Figs. 1(a) and 1(b)] is formed by a stack of tungsten, alumina, GeTe, and alumina deposited on a 100 nm aluminum nitride (AlN) underlayer, which serves as an electrical insulation layer and prevents current leakage from the heater to the silicon substrate. A 50 nm thick bow-tie shape W heater, which is used to induce the phase change of GeTe through Joule heating, is patterned on top of the AlN layer. The functional GeTe block is chosen to be 180 nm thick and is deposited by co-sputtering Ge and Te, and the composition is characterized to be 46:54. A mechanically compliant enclosure of 30 nm of refractory alumina, deposited by atomic layer deposition (ALD), surrounds the GeTe volume (deposited as two different layers) to direct and constrain the mechanical deformation during the phase change process. The use of alumina also mitigates the oxidation of the W heater and prevents interlayer diffusion at high temperatures as suggested by the Ellingham Diagram. Ground signal ground (GSG) probe pads are designed to apply the heating signal to the test structures using microwave probes that can maintain high speed pulse integrity. Complementary devices were also fabricated in which the GeTe functional volume has two extended electrical connections made by crystalline GeTe and connected to W pads to allow periodic electrical characterization of the PCM during cycling [Fig. 1(c)]. The high resistance contrast between the two phases is used as an indication of phase change and to determine the minimum power to amorphize (MPA) and the minimum power to crystallize (MPC) for each cell before the endurance cycling test.

A finite element analysis (FEA) model is constructed to simulate the device behavior and facilitate the structure design. The model uses experimentally measured material properties and thermal boundary resistance between AlN and W (see S1 of the supplementary material), which is one of the most critical parameters in setting the device temperature profile. Although other TBRs are present in the structure, their effect is negligible in determining the steady state temperature of the GeTe as the thermal path above the heater is dominated by the GeTe layer itself. The temperature profile discrepancy between the simulation and experiment results derived from the W thermometer is 11%. Primary results suggest that net actuator displacement and absolute height change are related to the void formation and growth that is observed in the endurance test.

There are many reported factors that could induce voids inside the PCMs, such as electrical field $^{16-18}$ or temperature gradient 19,20 induced element segregation subsequently leading to void formation or dewetting forces. We designed structures where GeTe and heater have different dimensions to examine the potential factors. The test cells are indexed according to the heater size and GeTe width. For example, if the heater is $6 \times 2 \, \mu \text{m}$ and the GeTe on top of it is $2 \, \mu \text{m}$ wide, the cell will be labeled as "W2L6-G2" [Fig. 1(c)]. To examine dewetting effects, we compare W1L6-G1 cells where the GeTe is fully melted during the crystalline to amorphous transition, and W1L6-G2 cell where the volume of the GeTe is melted only on top of the heater

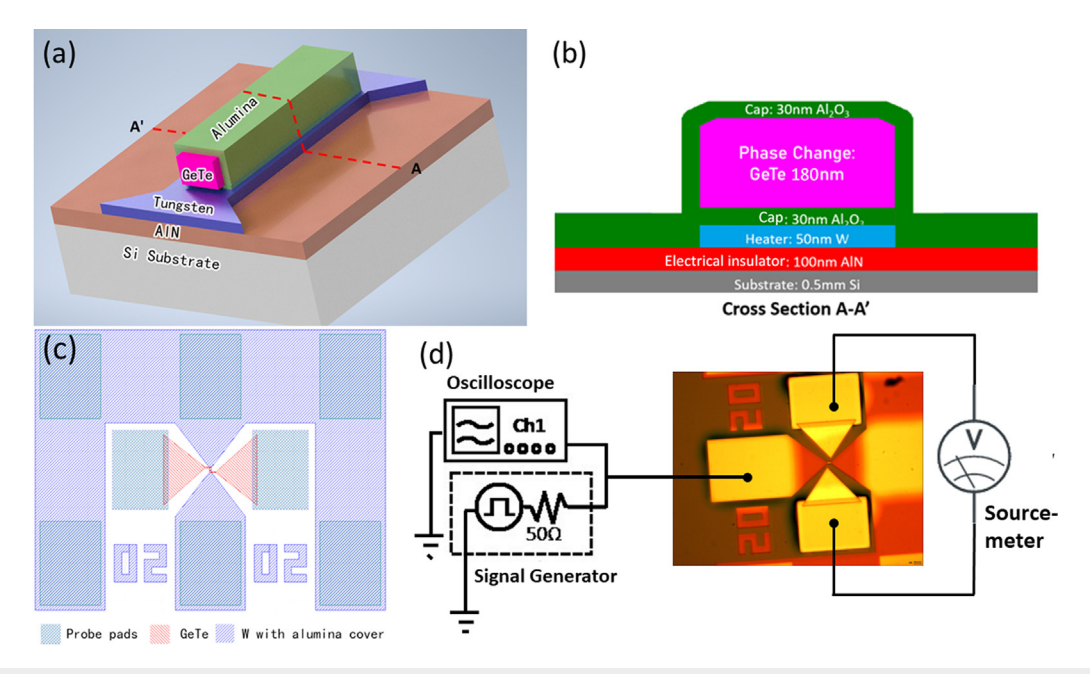


FIG. 1. The basic test structure: (a) 3D model of the test structure. The drawing aims to show all the materials in the structure. The GeTe layer is fully encapsulated in the actual device; (b) cross-sectional view of the device with all the material stacks and corresponding thickness; (c) W2L6-G2 cell layout with the $6 \times 2 \mu m^2$ heater size and $2 \mu m$ wide GeTe; (d) Test circuit setup for a W2L6-G2 cell with the two electrical connections.

the remaining unmelted GeTe acts as an anchor for the molten regions. To examine the temperature gradient effect, the heater size was varied while keeping the GeTe volume the same. This approach permits to test the effect of temperature gradient in the range from 2.3×10^8 to 2.2×10^7 K/m (see S2 of the supplementary material). Although the electric field can affect element segregation and void formation, the electric field inside the connection paths associated with the resistance measurement is about 1 V/cm, and its impact on the material is negligible.

The test equipment setup includes an Agilent 81110A pulse generator, an Agilent DSO70212B oscilloscope, connected through a Tadaptor to the heater with GSG probes, and a separate Keithley 2401 source-meter connected to the electrical connection pads with two DC probes [Fig. 1(d)]. The pulse generator supplies a voltage pulse to the heater which induces the GeTe phase change, while the oscilloscope detects the heater electrical response to the input pulses. The voltage response is not only used to monitor the heater behavior but also can be used as a thermometer based on the measured W heater thermal coefficient of resistance (TCR).²¹ The source-meter is used to measure the GeTe resistance, which shows the state of the GeTe, and detects the failure of devices. A MATLAB program is written to control the pulse generator and source-meter operation. It allows sequential operation of the tools and prevents signal crosstalk. In the programmed endurance test, a 300 ns MPA pulse is applied first to transform c-GeTe to a-GeTe, followed by a 1.5 μ s MPC pulse that transforms a-GeTe back to c-GeTe. The average MPA for W1L6-G1 and W2L6-G2 cells are 73.7 and 100.7 mW, respectively, and the average MPC for W1L6-G1 and W2L6-G2 cells are 29.9 and 32.1 mW, respectively. A 25 ms delay in between the pulses allows devices to reach a thermal equilibrium before the next phase change. Thus, one operation cycle takes about 50 ms without the source-meter measurement. The source-meter is turned on to measure the GeTe resistance after an MPA pulse or a MPC pulse, after the pulse generator has completed pulsing. Scanning electron microscopy (SEM) and atomic force microscopy (AFM) are used to check the test cell intermediate states at 1,10, 100, 1000, and 10 000 cycles for better understanding of the cap deformation and voiding behavior. Transmission electron microscopy (TEM) is applied to cycled devices for understanding the cross-sectional structure and element stoichiometry using Energy dispersive x-ray spectroscopy (EDS). 100 nm thick sample slices are prepared via Focus Ion Beam (FIB).

The endurance test is focused on test cells W1L6-G1 and W2L6-G2. The voltage responses of all the heaters remain the same during the test, meaning that the heat supply is not a variable. AFM results of the W1L6-G1 cell after a cycle where the GeTe stays in the crystalline state show the cap absolute height increases with cycling [Fig. 2(a)]. After 10,000 cycles, the cap absolute height increment reaches 45.6% on average compared with the initial height. The encapsulated volume is computed by integrating AFM data of the tested cells at the initial state and after 10 000 cycles. The comparison shows 21.9% volume change on average for three W1L6-G1 tested samples (see S3 of the supplementary material). The extra volume is coming from large voids captured by the SEM images. The SEM results also show the void formation and aggregation process [Figs. 3(a)-3(d)]: small voids first appear randomly inside the GeTe functional volume within the first few cycles, and with the cycle number increasing, small voids aggregate to form larger ones and migrate to the boundary of the device. The void aggregation is also suggested by the increase in resistance of the amorphous state GeTe [Fig. 3(e)]. The material agglomerates toward the center of the structure due to voiding and narrows the electrical conduction path. Thus, the continuous absolute height change can be explained via the agglomeration of GeTe toward the center of the cell.

In addition to this one-way trend with cycling of the actuator position when crystalline, the net actuator displacement between a-GeTe and c-GeTe was also extracted from the AFM results, which represents the useful stroke of the actuator. This net actuator displacement between a-GeTe and c-GeTe is 9.5 nm on average, excluding extreme values. On top of this average behavior, much large actuation is sporadically observed at certain cycles in the endurance test and reaches 44 nm on average [Fig. 2(b)]. Thus, the amount of actuation is much greater than the 8% expected from the phase change. From the intermediate state observation, the large net displacement occurs when

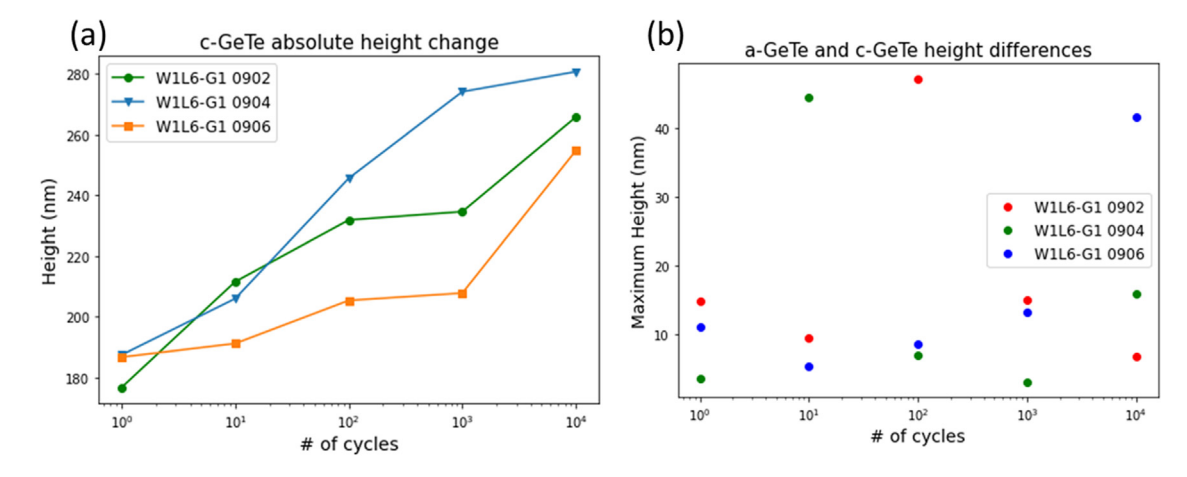
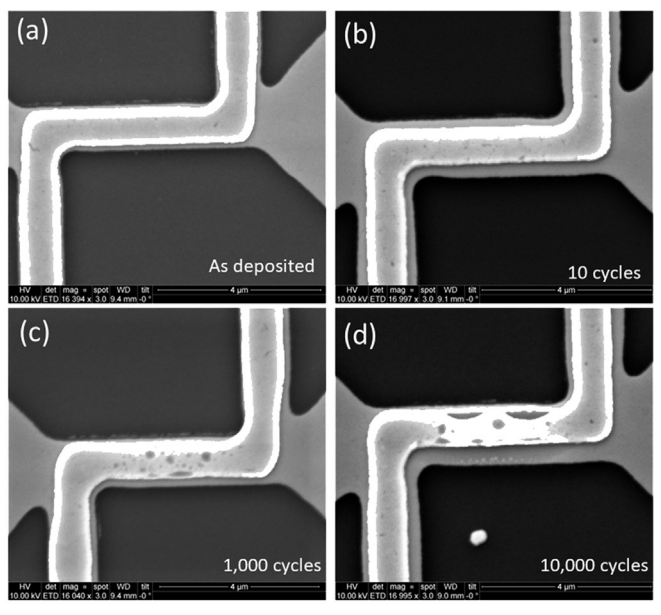


FIG. 2. Endurance test results of W1L6-G1 type devices: (a) AFM results about the absolute height change of the alumina cap in the c-GeTe state going from 1 to 10 000 cycles. The absolute height is obtained from averaging the peak value with its nearest three data points of each height profile. Further details about post-processing of these data are reported in S3 of the supplementary material. A continuous increment in displacement can be detected. (b) AFM results on the net displacement changes of the functional volume between the a-GeTe and c-GeTe. The maximum height change reaches 47 nm. Except the occasional large change, the height change is on average 10 nm.



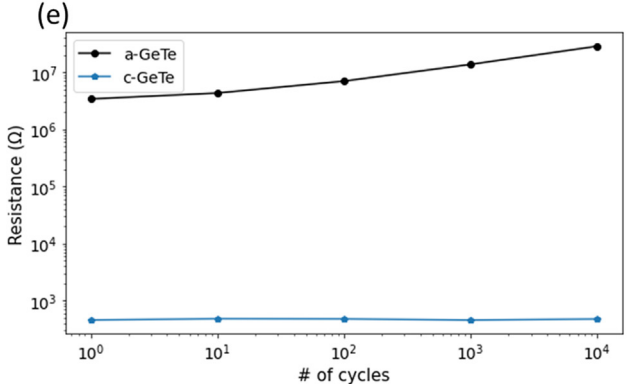


FIG. 3. SEM images of void formation and growth: (a) as-deposited state where no voids are visible; (b) after 10 cycles where small voids start to appear; (c) after 1000 cycles where more voids appear and start aggregating; (d) after 10 000 cycles where voids aggregate to form larger voids at the sides of the device; (e) resistance change of the functional GeTe volume in both crystalline state and amorphous state after 10, 100, 1000, and 10 000 cycles. The voiding has less effect on the crystalline state resistance due to the intrinsic low resistivity of the material, while it shows a clear impact on the amorphous state resistance when the GeTe aggregated toward the center of the structure and overall resistance increased an order of magnitude with cycling.

both agglomeration of GeTe and the phase change volume expansion participate in the actuation cycle. Once the voids aggregation finishes, net actuator displacement falls back to the lower steady state value.

The void formation and aggregation observed from the tested devices are similar to the thermally activated dewetting process (sometime referred to as agglomeration) which usually includes void nucleation and subsequent void growth.^{22,23} The formation of large voids and their migration to the boundary can be explained if the phenomenon is understood as dewetting. First, the voids nucleate from the inherent voids²⁴ and randomly appear inside the GeTe as shown in Fig. 3(b). Then, small voids start to aggregate and reduce the contact

area with the cap. Voids aggregates at the two edges of the actuator, reducing the effective contact area between GeTe and alumina. This, in turn, minimizes the total energy of the free surfaces and subsequently lowers the free energy of the system. As the voids continue to build up with cycling due to dewetting and the GeTe agglomerates toward the center, net displacement in the GeTe thickness can exceed 8% of the GeTe volume change, leading to the large actuation in our test devices. TEM results on the cross section of W2L6-G2 devices after 1000 cycles and 10000 cycles [Figs. 4(a) and 4(b)] show that all the voids locate only at the interface between the alumina and the GeTe which supports the dewetting assumption. Tests on the W1L6-G2 devices also validate the results. Thermal simulation has suggested that unlike the fully melted W1L6-G1 device, the W1L6-G2 cell has only part of the GeTe material melted with the same power applied. This would change the boundary at the side from "molten GeTealumina" to "molten GeTe-solid GeTe." We hypothesize that GeTe will not dewet from itself, and, therefore, the large voids seen in Fig. 3(d) will not appear at the sides but will appear in the center where the GeTe is in contact with alumina. The SEM result of W1L6-G2 both with and without electrical contact behaves as predicted [Figs. 4(c) and 4(d)] after 10 000 cycles.

To further confirm that dewetting exists between the alumina cap layer and the GeTe, we have conducted a screening test by depositing 200 nm GeTe on top of 30 nm alumina [Fig. 5(a)] and treated these samples with rapid thermal annealing (RTA) from 300 to 700 °C under an N2 atmosphere. The results of the experiment clearly show dewetting happening between the GeTe and alumina, with the process accelerating with increasing temperature. The experimental results for the samples heated to 400 °C via RTA for different dwell times going from 1 to 10 min [Figs. 5(b)-5(e)] show the process of dewetting of GeTe from alumina. The dewetting process follows the so-called "hole growth" method,²⁵ where a hole, or void, of a critical size starts to grow and because of capillary energy driven retraction, mass starts to accumulate at the edge of the hole to form a rim and nearby valley. The edge retracts with time such that the rim height increases, and the valley deepens to the point of pinch-off, which results in the formation of an island and a new hole edge. The final shape of the islands depends on the distance between holes, and in the case of GeTe and alumina, the non-circular shape indicates a fractal growth mode. This happens because the initial voids are sparse and the rims of the growing voids breakup into strands, which subsequently leads to the formation of non-circular islands.²³ In addition, the dewetting happens at a temperature lower than the melting temperature starting at around 400 °C, suggesting that the co-sputtered GeTe film is in a metastable state and can start to dewet in its solid state. Molten state dewetting can hardly be seen from the test because without any proper encapsulation, GeTe melts and evaporates away from the substrate.

There are other factors than the dewetting force that contribute to the void formation. The temperature gradient as the most pronouncing factor has been examined on similar geometries. The stoichiometry of Ge and Te of the device after 1000 and 10 000 cycles obtained from EDS suggests small element segregation with less than 10% concentration change, which is less than what would be expected given the element thermal diffusivity in the melting state when a 10⁸ K/m temperature gradient is present¹⁹ and shows no indication of the segregation driven void formation (see S4 of the supplementary material). Therefore, we

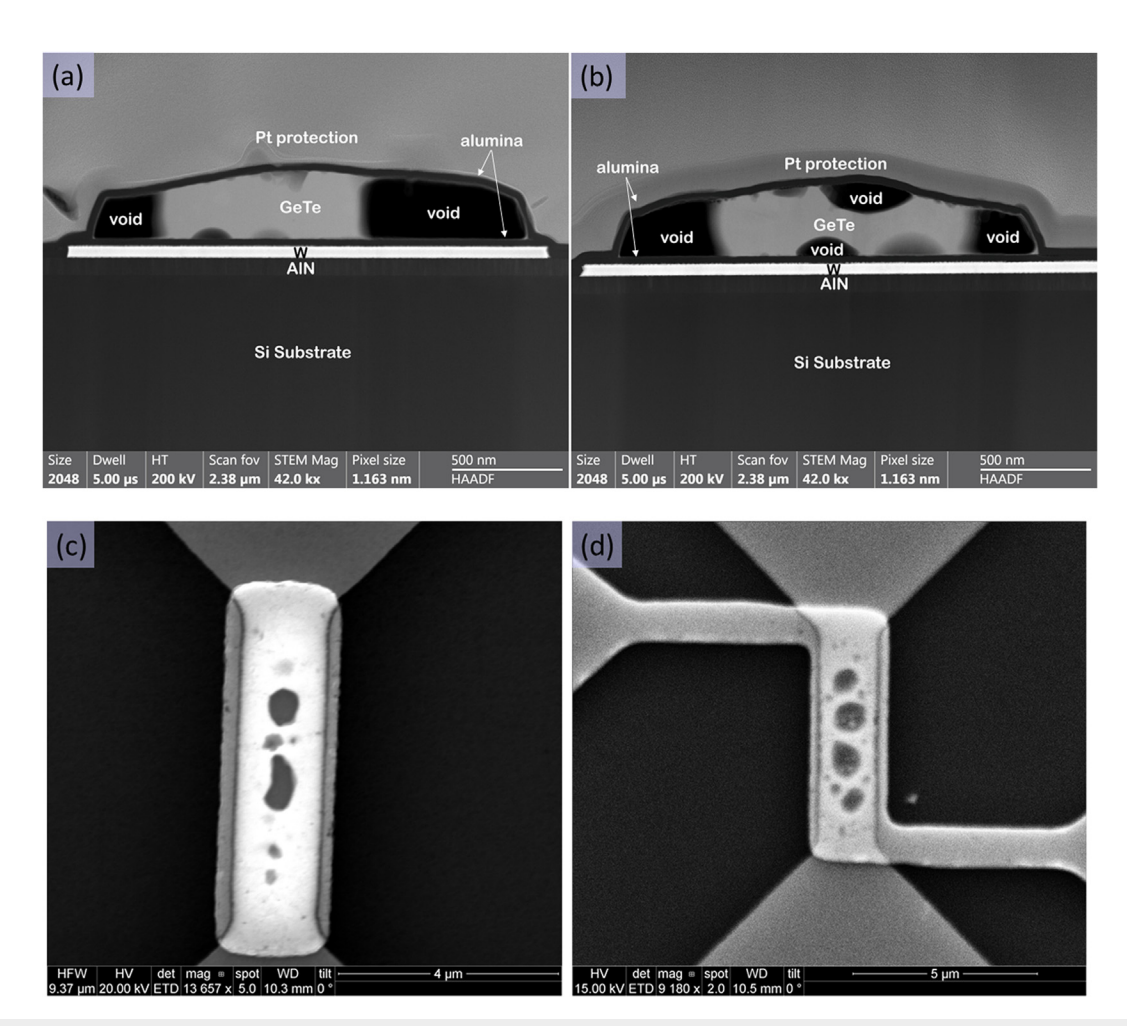


FIG. 4. Evidence of dewetting between alumina and GeTe. (a) Dark-field TEM image of cross-sectional AA' view of the W2L6-G2 #0602 cell after 1000 cycles. (b) Dark-field TEM image of cross-sectional AA' view of the W2L6-G2 #1002 cell after 10 000 cycles where all the voids locate between alumina and GeTe boundary. SEM images showing similar void formation despite varying mechanical boundary conditions for the melting GeTe: (c) W1L6-G2 cell with no electrical connection after 10 000 cycles showing all the voids at the center (d) W1L6-G2 cell with electrical connection showing similar results after 10 000 cycles where the voids only aggregate to the center with no large voids at the sides.

conclude that dewetting is the main driving force for the devices reported herein.

The controlled experiment between W1L6-G1 cells and W2L6-G2 cells indicates that a stiffer cap confinement can suppress the dewetting effect. Based on its geometry, the W1L6-G1 cap flexural rigidity is expected to be four times greater than the W2L6-G2 cap, and as compared in S5 of the supplementary material, the formation and aggregation of voids require longer time in W1L6-G1 cells. We attribute this result to requiring greater energy to deform a more rigid cap. The longer aggregation time directly impacts the life cycle of the W1L6-G1 cell, which is greater than that of the W2L6-G2 cell. The life cycle of the W1L6-G1 cell, on average, reaches 360 000 cycles and achieves a maximum of 1×10^6 cycles in some cases. This is substantially larger than the life cycle of the W2L6-G2 cells, which usually fails before 100 000 cycles. The failure is mainly caused by agglomeration of GeTe toward the device center, producing a deformation stress inside the cap that exceeds the alumina breaking point, which leads to

cracking of the cap and GeTe leakage. Both SEM images and electrical characterization of the open circuit condition support this mechanism (see S6 of the supplementary material). The capping material has the same thickness for all the cells; thus, the longer device life cycle means longer time is needed for the cap deformation, caused by GeTe agglomeration due to dewetting, to reach its failure point. These same results also indicate a reduction of dewetting driven material motion with a more rigid cap.

In summary, we have identified a phenomenon of the PCM interaction with the capping alumina material. The dewetting between GeTe and alumina dominates the device behavior, leading to void formation and growth, and the agglomeration of GeTe, minimizing contact area and reducing the system energy. Dewetting can generate large forces that drive the net actuator displacement to reach 24.7% of the initial height, greater than the 8% expected from density change between two phases. However, the absolute height also continuously increased through cycling since no constraint is added to impede the

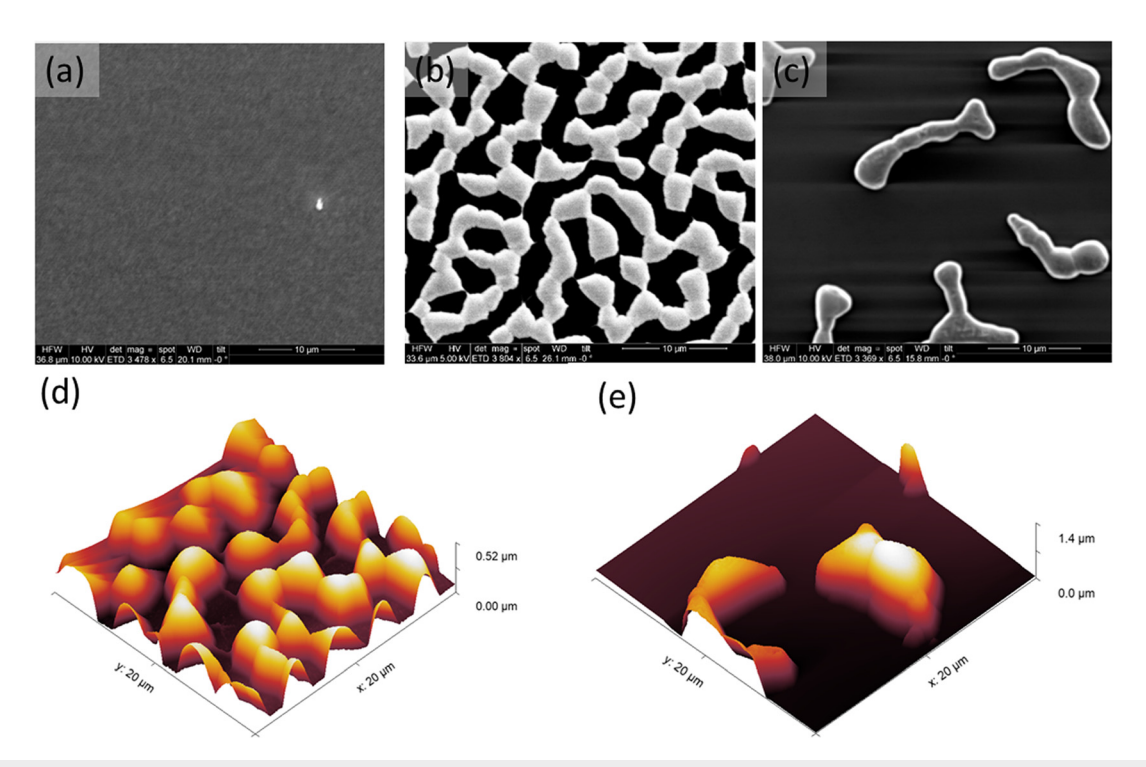


FIG. 5. Fractal growth mode of 200 nm GeTe on 30 nm alumina from the RTA test. (a) SEM image of as-deposited GeTe; (b) SEM image of GeTe after 400 °C RTA for 1 min; (c) SEM image of GeTe after 400 °C RTA for 10 min; (d) AFM image of GeTe after 400 °C RTA for 1 min—the average particle height is 402 nm; and (e) AFM image of GeTe after 400 °C RTA for 10 min—the average particle height is 1151 nm.

dewetting process, which leads, eventually, to the breaking of the cap and failure of the device in the end. Experiments have shown that having stiffer confinement structures can suppress the dewetting progress and extend the device endurance. Further improvement of the structure needs to be studied to help control the phenomenon and benefit from the large displacement this class of nanoscale actuators can produce.

See the supplementary material for additional information on critical material parameter characterization, thermal and mechanical simulation details, AFM data processing technique, evolution of voids in different cells, GeTe stoichiometry analysis, and failure characterization.

The authors gratefully acknowledge the financial support from the National Science Foundation for the project (LEAP-HI joint project: Ultra-Low Power Computing: A Disruptive Approach Through a New Integrated Nanomechanics Framework) under Grant No. CMMI-1854702. They would also like to thank Maarten de Boer, Luis Hurtado from CMU; Robert Carpick, Andrew Rappe, GÖKHAN ŞENSOY, and Cangyu Qu from UPenn; and David Srolovitz from HKU for useful discussion.

AUTHOR DECLARATIONS Conflict of Interest

The authors have no conflicts to disclose.

Author Contributions

Xinyi Fang: Conceptualization (equal); Data curation (equal); Formal analysis (equal); Investigation (equal); Methodology (equal); Software (equal); Visualization (equal); Writing – original draft (equal); Writing – review & editing (equal). Mohammad Ayaz Masud: Methodology (equal); Software (supporting). Gianluca Piazza: Conceptualization (equal); Funding acquisition (equal); Project administration (equal); Resources (equal); Supervision (equal); Writing – review & editing (equal), Resources (equal); Supervision (equal); Writing – review & editing (equal).

DATA AVAILABILITY

The data that support the findings of this study are available from the corresponding authors upon reasonable request.

REFERENCES

¹M. Wuttig and N. Yamada, Nat. Mater. 6, 824 (2007).

²H. Zhang, L. Zhou, J. Xu, N. Wang, H. Hu, L. Lu, B. M. A. Rahman, and J. Chen, Sci. Bull. 64, 782 (2019).

³Z. Cheng, C. Ríos, N. Youngblood, C. D. Wright, W. H. P. Pernice, and H. Bhaskaran, Adv. Mater. 30, 1802435 (2018).

⁴M. Wuttig, H. Bhaskaran, and T. Taubner, Nat. Photonics 11, 465 (2017).

⁵C. Wu, H. Yu, S. Lee, R. Peng, I. Takeuchi, and M. Li, Nat. Commun. **12**, 96 (2021)

⁶H. S. P. Wong, S. Raoux, S. Kim, J. Liang, J. P. Reifenberg, B. Rajendran, M. Asheghi, and K. E. Goodson, Proc. IEEE 98, 2201 (2010).

- ⁷T. Tuma, A. Pantazi, M. LeGallo, A. Sebastian, and E. Eleftheriou, Nat. Nanotechnol. 11, 693 (2016).
- ⁸W. Zhang, R. Mazzarello, M. Wuttig, and E. Ma, Nat. Rev. Mater. 4, 150 (2019).
- ⁹W. S. Khwa, K. Akarvardar, Y. S. Chen, Y. C. Chiu, J. C. Liu, J. J. Wu, H. Y. Lee, S. M. Yu, C. H. Lee, T. C. Chen, Y. C. Lin, C. F. Hsu, T. Y. Lee, T. K. Ku, C. H. Kuo, J. Y. Wu, X. Y. Bao, C. S. Chang, Y. D. Chih, H. S. P. Wong, and M. F. Chang, in *Symposium on VLSI Technology* (IEEE, 2021).
- ¹⁰G. Slovin, M. Xu, R. Singh, T. E. Schlesinger, J. Paramesh, and J. A. Bain, IEEE Trans. Microwave Theory Tech. 65, 4531 (2017).
- $^{11}\mathrm{M}.$ Wang and M. Rais-Zadeh, J. Micromech. Microeng. 27, 013001 (2017).
- ¹²M. Gallard, M. S. Amara, M. Putero, N. Burle, C. Guichet, S. Escoubas, M. I. Richard, C. Mocuta, R. R. Chahine, M. Bernard, P. Kowalczyk, P. Noé, and O. Thomas, Acta Mater. 191, 60 (2020).
- ¹³J. Best and G. Piazza, in *IEEE International Conference on Micro Electro Mechanical Systems (MEMS)* (IEEE, 2019), p. 962.
- ¹⁴R. Cheng, Y. Ding, S. M. Koh, Y. Yang, F. Bai, B. Liu, and Y. C. Yeo, IEEE Trans. Electron Devices 61, 2647 (2014).
- ¹⁵J. T. Best, M. A. Masud, M. P. deBoer, and G. Piazza, Adv. Electron. Mater. 8, 2200085 (2022).

- ¹⁶D. Kang, D. Lee, H. M. Kim, S. W. Nam, M. H. Kwon, and K. B. Kim, Appl. Phys. Lett. **95**, 011904 (2009).
- T. Y. Yang, I. M. Park, B. J. Kim, and Y. C. Joo, Appl. Phys. Lett. 95, 032104 (2009).
 A. Padilla, G. W. Burr, C. T. Rettner, T. Topuria, P. M. Rice, B. Jackson, K. Virwani, A. J. Kellock, D. Dupouy, A. Debunne, R. M. Shelby, K. Gopalakrishnan, R. S. Shenoy, and B. N. Kurdi, J. Appl. Phys. 110, 054501 (2011).
- ¹⁹P. Yeoh, Y. Ma, D. A. Cullen, J. A. Bain, and M. Skowronski, Appl. Phys. Lett. 114, 163507 (2019).
- ²⁰A. Debunne, K. Virwani, A. Padilla, G. W. Burr, A. J. Kellock, V. R. Deline, R. M. Shelby, B. Jackson, B. Jackso, and J. Electrochem, Soc. Society 158, H965–H972 (2011).
- ²¹M. Xu, G. Slovin, J. Paramesh, T. E. Schlesinger, and J. A. Bain, Rev. Sci. Instrum. 87, 024904 (2016).
- ²²P. R. Gadkari, A. P. Warren, R. M. Todi, R. V. Petrova, and K. R. Coffey, J. Vac. Sci. Technol. A 23, 1152 (2005).
- ²³J. A. Diez, A. G. González, D. A. Garfinkel, P. D. Rack, J. T. McKeown, and L. Kondic, Langmuir 37, 2575 (2021).
- ²⁴Z. Sun, J. Zhou, A. Blomqvist, B. Johansson, and R. Ahuja, Phys. Rev. Lett. **102**, 075504 (2009).
- ²⁵C. V. Thompson, Annu. Rev. Mater. Res. **42**, 399 (2012).